LBL-18688
Preprint c.2

Lawrence Berkeley Laboratory
UNIVERSITY OF CALIFORNIA

RECEIVED
LAWRENCE
BERKELEY LABORATORY
JAN 9 1985
LIBRARY AND
DOCUMENTS SECTION

Submitted to Nuclear Physics

SEQUENTIAL FISSION ANGULAR DISTRIBUTIONS FROM
MASS-ASYMMETRIC HEAVY ION REACTIONS

D.J. Morrissey, G.J. Wozniak, L.G. Sobotka,
R.J. McDonald, A.J. Pacheco, and L.G. Moretto

November 1984

Prepared for the U.S. Department of Energy under Contract DE-AC03-76SF00098

LBL-18688 c.2

DISCLAIMER

This document was prepared as an account of work sponsored by the United States Government. While this document is believed to contain correct information, neither the United States Government nor any agency thereof, nor the Regents of the University of California, nor any of their employees, makes any warranty, express or implied, or assumes any legal responsibility for the accuracy, completeness, or usefulness of any information, apparatus, product, or process disclosed, or represents that its use would not infringe privately owned rights. Reference herein to any specific commercial product, process, or service by its trade name, trademark, manufacturer, or otherwise, does not necessarily constitute or imply its endorsement, recommendation, or favoring by the United States Government or any agency thereof, or the Regents of the University of California. The views and opinions of authors expressed herein do not necessarily state or reflect those of the United States Government or any agency thereof or the Regents of the University of California.

Sequential Fission Angular Distributions from Mass-Asymmetric Heavy Ion Reactions

D. J. Morrissey

National Superconducting Cyclotron Laboratory

and Department of Chemistry

Michigan State University

East Lansing, MI 48824-1321

G. J. Wozniak, L. G. Sobotka*, R. J. McDonald,

A. J. Pacheco+, and L. G. Moretto

Nuclear Science Division

Lawrence Berkeley Laboratory

Berkeley, CA 94720

work was supported, in part, by the Director, Office of Energy Research, Division of Nuclear Physics of the Office of High Energy and Nuclear Physics of the U.S. Department of Energy under Contract DE-AC03-76SF00098, and by the National Science Foundation under Grant No. PHY 80-17605.

Abstract:
The angular distributions of sequential fission fragments have been measured for the reactions of ^{40}Ar with ^{197}Au and ^{238}U as a function of reaction Q-value and charge transfer. These angular distributions are used to study the angular momentum and alignment of the deep-inelastic products which undergo fission. All of the fission fragment angular distributions are strongly focused into the plane defined by the beam and the projectile-like fragment velocity vectors. The in-plane angular distributions from reactions with uranium are isotropic for small energy losses and become anisotropic as the energy loss increases. For large negative Q-values, the in-plane anisotropy increases as the deep-inelastic products become more symmetric. The variation of the in-plane anisotropy with mass asymmetry for the two systems in this work was compared to a compilation of previous work and a consistent pattern was found. These alignment data are compared to equilibrium statistical calculations.

NUCLEAR REACTIONS: ^{197}Au, ^{238}U (^{40}Ar, HI f) E=340 MeV; measured sequential fission angular distributions $W(\Theta,\Phi)$, in-plane and out-of-plane. Angular distribution functions, deduced spin transfer, spin alignment. Systematics of previous work. Equilibrium statistical model.

---

1. Introduction

When a compound nucleus fissions, a large amount of information on its intrinsic spin is contained in the angular distribution of the fission fragments [1]). This fact has been applied to sequential fission following deep-inelastic scattering in order to determine the magnitude and orientation of the spin of the deep-inelastic fragments [2-4]). Measurements of the angular distributions of alpha particles [5]), continuum gamma-rays [6]), discrete gamma-rays [7]) and the circular polarization of gamma-rays [8]) from the fragments have also been undertaken in order to determine the magnitude, polarization and the alignment of the angular momentum. Each of these techniques is more suited to a specific aspect of the spin distribution, so that a more complete picture can be constructed by using all of these complementary approaches.

The out-of-plane distribution of fission fragments is sensitive to both the magnitude and alignment (P_{zz}) of the spin. The in-plane angular distributions of sequential fission fragments can yield information on the in-plane components of the angular momentum (P_{xy}). This aspect is not readily accessible with the other techniques. Measurements of sequential fission angular distributions [2-4,9,10]) have shown that sizable in-plane anisotropies are seen, provided that the deep-inelastic collision is well characterized, i.e. not integrated over a broad range of any variable. Thus, sequential fission can be used to measure the difference among the components of the spin generated in a deep-inelastic collision.

Several models predict the distribution of the three spin components of deep-inelastic products [11-16]) . Such models range from the limit of statistical equilibrium applied to the degrees of freedom of the

dinuclear complex [11,12]) to dynamical calculations of the intrinsic spins of the fragments from either the excitation of surface vibrations [13]) or from particle transfer [14-16]).

In particular, the statistical equilibrium model predicts an increasingly anisotropic misaligment due to an increasing angular momentum projection along the line-of-centers with increasing mass asymmetry [9]). The qualitative reason for this effect is the following. The mode corresponding to the tilting of the dinuclear axis away from the normal to the total angular momentum becomes "softer" with increasing mass asymmetry [12]). This softening with increasing mass asymmetry is due to the fact that the moments of inertia with respect to the axis parallel and perpendicular to the line-of-centers are equal in the limit of infinite mass asymmetry. Consequently, at any given temperature, the tilting mode becomes more excited with increasing mass asymmetry.

We have studied the alignment of the angular momentum created in the fragments from deep-inelastic collisions with two systems for which the statistical equilibrium model predicts a significant change in the alignment over the range of reaction products. Such measurements can provide systematic data for comparison to the model predictions.

In this paper we report measurements of sequential fission angular distributions from the reaction of 340 MeV ^{40}Ar with ^{197}Au and ^{238}U. The experimental details of this work are presented in section 2, including a brief discussion of the data analysis. The results are presented in section 3 in the form of fission fragment angular distributions. These data are fit to theoretical angular distribution functions and are discussed in section 4. Additional information from previous studies of sequential fission is combined with the present work in order to obtain

the overview of sequential fission in deep-inelastic collisions presented in section 5.

2. Experimental

The experimental technique used in the present study is the same as that used in a previous work [9]) and will be described here briefly. A 340 MeV ^{40}Ar beam from the SuperHILAC at the Lawrence Berkeley Laboratory was used to irradiate a 1.0 mg/cm^2 gold foil and subsequently a 0.92 mg/cm^2 uranium fluoride deposit on a 0.52 mg/cm^2 aluminum backing. The beam current was monitored with a current integrator connected to a secondary-electron-suppressed Faraday cup. The beam current was held constant at approximately 20 electrical nA to maintain a reasonable ratio of real-to-random events. The target was placed in a holder that allowed for the motion of the target in two perpendicular planes, and was oriented in such a way as to balance the energy loss corrections made to the energies of the reaction products. These corrections were important because products were detected on both sides of the beam axis in as well as out of the scattering plane.

Projectile-like fragments (PLF) were detected in a gas ionization telescope which was able to resolve nuclear charges up to approximately Z=30 [17]). The mass of the PLF was obtained in an iterative calculation described below. The solid angle of the PLF telescope was defined to be 3 msr by a copper collimator on the 300 micron Si surface barrier E detector. The energy response of the telescope was calibrated by elastically scattering 340., 293.5, 239.5, and 178.5 MeV ^{40}Ar ions from a ^{197}Au target. During the coincidence measurements, the telescope remained fixed at an angle near the classical grazing angle for each target, 40° for gold, and 45° for uranium.

Coincident fission fragments (FF) were detected on the opposite side of the beam from the PLF in an array of 8 Si surface barrier detectors. The array of FF detectors was fixed to a common support and moved in unison. In general, four FF detectors were in-plane and four were out-of-plane with respect to the beam axis and the PLF velocity vector. The detectors were moved to cover the range between 50° and 155° in-plane and between 15° and 90° from the normal out-of-plane. The solid angles of the FF detectors were defined by electropolished rings and measured with a known ^{241}Am standard. The solid angle of each FF detector was found to be 7.3 msr within 5 percent. The energy calibrations of the FF detectors were obtained with alpha particles from ^{212}Pb and ^{241}Am sources in conjunction with a linear pulser.

All events with a coincidence between a PLF and any fission detector plus a scaled-down fraction of the PLF inclusive events were written onto magnetic tape for off-line analysis. The raw data was passed through a filtering code that collected all the coincidence events in a condensed form on a magnetic tape along with several representative tapes of PLF inclusive events. After this point the data reduction followed two paths. The inclusive data were used to check the run-to-run normalization of the beam current and to obtain PLF inclusive data for the calculation of the fission probabilities.

The coincidence data were transformed into the rest frame of the recoiling target-like fragment (TLF) as previously described in detail[9]). Briefly, the data were transformed on an event-by-event basis and angular distributions were constructed in the rest frame of the target-like nucleus after the conversion. This transformation relies on the measurement of the charge and energy of the PLF, and on the knowledge of the laboratory scattering angle, along with the assumption of two body

kinematics in the primary scattering process. The kinetic energy of the PLF was corrected for energy losses in the target and in any other absorbers [18]) back to the midpoint of the target. The calibration of the telescope with elastically scattered ^{40}Ar particles at several beam energies automatically included the pulse-height defect of the PLF. The atomic number of the PLF was determined exactly in the range 9 to 30 over the entire energy region of interest. The mass of the PLF was calculated by assuming neutron to proton equilibrium in the dinuclear complex followed by an iterative correction for neutron emission. This correction assumed a constant velocity of the emitting nuclei and a partition of the excitation energy in proportion to the mass. The large mass asymmetry in both reactions forced this iterative correction to be small and to converge quickly.

The energy of the FF was corrected for the energy loss in the target [18]) and for the pulse-height defect [19]) in the Si detector by assuming that the mass and charge of the fission fragment were half that of the heavy reaction partner. This assumption was also necessary in order to calculate the FF momentum vector used to transform the event into the rest frame of the TLF. The transformed FF energy distributions from reactions with ^{197}Au were found to be approximately Gaussian in shape. The FF energies from reactions with ^{238}U were also Gaussian shaped in-plane. However, fig. 1 shows that these FF energy distributions became narrower and developed a minimum for decreasing values of Θ. (The usual spherical polar coordinates are used throughout this paper with $\Theta=0$ perpendicular to the plane of the scattering event.) The appearance of a minimum indicates that lower excitation energy fission events (mass asymmetric FF) are associated with sequential fission of nuclei with lower angular momentum (less preference for emission in the reaction

plane). The centroids of the FF energy distributions were peaked at values that are consistent with the Viola systematics [20]) (e.g. single fragment energies of 70 MeV for gold and 85 MeV for uranium).

3. Results

Contours of the probability for detecting a sequential fission fragment from reactions with gold and uranium are shown in Fig. 2 as a function of total kinetic energy (TKE) and projectile-like fragment charge (Z_3). These probability contours change dramatically as one goes from gold to uranium, because the gold-like fragments have significantly higher fission barriers than the uranium-like fragments. The true fission probabilities can be obtained from the quantities presented in Fig. 2 by dividing them by the PLF inclusive cross section, $d^2\sigma/d\Omega dZ$. Fission probabilities are shown as a function of PLF charge in fig. 3 and as a function of TKE in fig. 4. Their qualitative behavior reflects the variation of the fission barriers and of the excitation energies with PLF charge. An important preliminary result is that a broad range of deep-inelastic reaction products are observed in coincidence with fission products from both targets when the energy loss is about 150 MeV.

The measured FF angular distributions are shown in figures 5 to 10. Both Φ^H, the in-plane angle, and Θ^H, the out-of-plane angle, are in the rest frame of the recoiling target-like nucleus with $\Phi^H = 0$ and $\Theta^H = 0$ corresponding to the laboratory recoil direction and the normal to the plane containing the deep-inelastic event, respectively. The error bars on the data points are obtained by combining the statistical error in the measurement with an assumed systematic error of 5 percent from the solid angle calibration. The data from the uranium target were divided in two different ways, into four Q-value bins (summed over PLF Z_3 values) and also into three Z_3 bins with Q-values between -100 and -200 MeV. The data

from the gold target were only divided into the latter Z_3 bins for the same range of Q-values due to the limited number of coincidences at small inelasticities. The curves drawn through the data in figs. 5 through 10 represent angular distribution functions that were fit simultaneously to the in-plane and out-of-plane data from each binning. The functional form of the angular distribution is discussed below.

Some systematic features of the angular distributions stand out at this point. All the angular distributions are strongly peaked in-plane (figs. 5 to 7) indicating that large amounts of angular momentum are present in the fissioning nuclei. The uranium data shows that the in-plane focussing increases as the inelasticity increases. This is an indication that the angular momentum of the fissioning nuclei is increasing with increasing inelasticity. The out-of-plane angular distributions for both systems become less focussed as the PLF charge increases. This behavior is in qualitative agreement with the rigid rotation prediction that the partition of the angular momentum is in proportion to the ratio of the moments of inertia of the primary reaction products.

The in-plane angular distributions from uranium (fig. 8) are isotropic at small inelasticities and become anisotropic at larger inelasticities. In the latter case, the angular distribution integrated over PLF charge (fig. 9) shows an in-plane anisotropy of approximately 1.4:1. The gold data in fig. 10 show a similar anisotropy. When the angular distributions are gated on PLF charge, as also shown in figs. 9 and 10, a strong variation of the in-plane anisotropy is seen with mass asymmetry. The anisotropy increases as the DIC fragments become more symmetric. This trend is apparently opposite to that predicted by the statistical equilibrium model for two touching spheres.[11,12]) However, in

section 5, it is shown that including deformation in the model calculations and correcting the experimental in-plane misalignments for differing amounts of spin in the fissioning nucleus gives good agreement between the calculations and all the data.

4. Discussion

A. Angular Distribution Functions

Analytical functions have been derived for in-plane and out-of-plane FF angular distributions by assuming a Gaussian distribution in the three angular momentum components[13,21-23]). Such Gaussian spin distributions are expected from very general statistical considerations. In the statistical model such a distribution is:

$$P(I_x, I_y, I_z) \propto e^{-\left\{ \left(\frac{I_x^2}{\sigma_x^2}\right) + \left(\frac{I_y^2}{\sigma_y^2}\right) + \left(\frac{(I_z - \bar{I}_z)^2}{\sigma_z^2}\right) \right\}} \qquad 1.$$

where I_z and $\bar{I}_z$ are the spin component and its average value aligned with the total angular momentum, I_y is the component along the dinuclear axis and I_x is the component along the axis orthogonal to the other two.

In the rest frame of the fissioning nucleus, the FF angular distribution that arises from such a spin distribution can be written as:

$$W(\Theta^H, \Phi^H) \propto \exp\{ - \langle I_z \rangle^2 \cos^2\Theta^H / 2\, S^2\} / S \qquad 2.$$

with

$$S^2 = 2K_0^{\,2} + \sigma_z^{\,2}\cos^2\Theta^H + \sin^2\Theta^H\, [\sigma_x^{\,2}\sin^2(\Phi^H - \Psi) + \sigma_y^{\,2}\cos^2(\Phi^H - \Psi)] \qquad 3.$$

where: $\langle I_z \rangle$ is the projection of the spin on the Z axis, $\sigma_x, \sigma_y, \sigma_z$ are the three Gaussian widths, $K_0^{\,2}$ is the variance of the projection of the total spin on the separation axis, and ψ is a shift angle. The last variable is

included because the symmetry axis of the dinuclear complex at scission does not necessarily coincide with the laboratory recoil direction ($\phi^H=0$). In a classical picture of the collision, the transfer of orbital angular momentum into intrinsic spin causes an angular shift of the symmetry axis away from $\phi^H=0$.

Broglia et al. pointed out that the fragment spin distribution is not completely determined by the observed FF angular distributions [13]. Harrach has emphasized that only three independent parameters can be determined by fitting an experimental angular distribution [24], excluding the overall normalization, by rewriting Eq. 2 in an alternate form that stresses this limitation:

$$W(\Theta^H,\phi^H) \propto \exp\{-q_2^2 \cos^2\Theta^H / 2R^2\} / R \qquad 4.$$

where now,

$$R^2 = 1 + q_3 \sin^2\Theta^H \cos[2(\phi^H-\Psi)] + q_4 \cos^2\Theta^H . \qquad 5.$$

The two expressions are related in the following manner:

$$q_2 = \langle I_z\rangle^2 / K^2_{eff} \qquad 6.$$

$$K^2_{eff} = K_0^2 + [(\sigma_x^2 + \sigma_y^2)/2] \qquad 7.$$

$$q_3 = (\sigma_y^2 - \sigma_x^2) / 2K^2_{eff} \qquad 8.$$

$$q_4 = [\sigma_z^2 - (\sigma_x^2 + \sigma_y^2)/2] / K^2_{eff} . \qquad 9.$$

These expressions are written in such a way that the parameters of the angular distribution, q_2, q_3 and q_4, can be obtained from the experimental data without knowledge of K_0^2 and $\langle I_z\rangle$ after the shift angle, Ψ, has been estimated with a model of the collision trajectory.

In some previous work [2-4]), the direction of the symmetry axis was assumed to coincide with the recoil direction of the TLF in the laboratory. This is only correct if the initial orbital angular momentum is nearly equal to the final orbital angular momentum. Our estimate of Ψ was obtained by tracing the path of the exit channel reaction products backward along a Coulomb trajectory to the scission configuration. These Coulomb trajectories were calculated for each Q-value bin of the data using estimates of the exit channel orbital angular momentum and a sphere-spheroid shape for the scission configuration of the deep-inelastic fragments as discussed in the Appendix. The variation of Ψ with TKEL is shown in fig. 11A. The symmetry axis of the dinuclear complex shifts rapidly away from the lab recoil direction at small energy losses, because the difference between the amount of angular momentum in the entrance and exit channels increases rapidly in this TKEL region.

B. Fitted Angular Distributions

Equations 4 and 5, were fit to all the experimental data for a given Q-value bin with a computer code that minimized the chi-square:

$$\chi^2 = \Sigma_i \, [W_{obs}(\Theta_i^H, \Phi_i^H) - W_{calc}(\Theta_i^H, \Phi_i^H) \, / \mathrm{Delta}(\Theta_i^H, \Phi_i^H) \,]^2 \qquad 10.$$

where $\mathrm{Delta}(\Theta_i^H, \Phi_i^H)$ is the error in the measured value, described above. The values of the fitted parameters are contained in Table I along with the reduced chi-square value of each fit. The uncertainties in the fitted values (given in parentheses) are those for which chi-square increased by one.

The dependence of the fitted values of q_2, q_3, and q_4 on the calculated value of the shift angle was estimated as follows. The length of the scission configuration used as the end point of the Coulomb trajectory was considered uncertain by 1 fm. Such an uncertainty leads to an uncertainty in Ψ of approximately 5° (a more compact scission

configuration leads to an angle closer to the laboratory recoil direction and thus to a smaller value of Ψ). When the angular distributions were fit with $\Psi \pm 5°$, the values of q_2 generally changed by 0.5 units (U data) and 1. unit (Au data); q_3 changed by 0.05 units (both data sets) and q_4 changed by 0.1 units (both data sets). The quality of the fits to the two angular distributions which are isotropic in-plane did not depend on the shift angle.

The dependence on TKEL of the parameters obtained by fitting the $^{40}Ar + ^{238}U$ angular distributions are shown in figures 11 B, C and D. These fitted parameters quantify the features of the angular distributions that we have already noted. All of these features of the FF angular distributions are similar to those observed in recently reported data[10]) for sequential fission from the very similar reaction of ^{40}Ar with ^{209}Bi.

The parameter, q_2, which is proportional to the square of the aligned spin, increases with TKEL and decreases as the charge of the PLF is increased. Such a decrease is consistent with the partition of a fixed amount of angular momentum in proportion to the moments of inertia. The value of q_3, proportional to the difference in the variances of the in-plane spin components, is small at low values of TKEL and larger at high values of TKEL. The value of q_3 also increases as the charge of the PLF increases, or as the charge division becomes more symmetric. This result is discussed below.

The statistical equilibrium model[11,12]) applied to an axially symmetric system predicts $\sigma_x = \sigma_z$ and thus $q_3 = -q_4$. Moreover, in this model q_3 should be positive and q_4 negative as σ_y should be greater than σ_z. This statistical equilibrium model prediction was tested by refitting the angular distributions to equations 4 and 5 with q_2 and q_3

as free parameters, with q_4 set equal to $-q_3$, and with the same values of Ψ. The results of such a constrained fit to the data are presented in Table II. The quality of the fits to the U data are, in general, comparable to those given in Table I. However, all the constrained fits to the Au data were significantly poorer than those in Table I.

An inspection of Table I indicates that the gold angular distributions might be better fit with both positive and similar values of q_3 and q_4. The results of another constrained fit with both q_3 and q_4 having positive and equal values are presented in Table III. These results are comparable to the unconstrained fits presented in Table I for both the Au and U data. For the U data, the similar chi-squared values obtained in the unconstrained and the two constrained fits demonstrate the relative insensitivity of these data to values of q_4. For the Au data, the similar chi-square values for the unconstrained and the fit with $q_3 = q_4 > 0$ indicate that σ_y is similar in magnitude to σ_z and that σ_x is somewhat smaller (where y,z and x are the line-of-centers, the total angular momentum and the axis orthogonal to the other two, respectively). This is in contrast to the expectation from the statistical equilibrium model that $\sigma_y > \sigma_x = \sigma_z$.

With the fitted values of q_2, q_3 and q_4 described above, one has three equations and five unknowns: K_0^2, $\langle I_z \rangle$, σ_x, σ_y and σ_z. The aligned spin of the fissioning nucleus can be determined in a model dependent way (see appendix) by using values of the σ's obtained from the equilibrium statistical model[11,12]), empirical values of K_0^2 and the fitted value of q_2. In Table V values of $\langle I_z \rangle$ that were extracted from the sequential fission angular distributions are shown. For the $^{40}Ar + ^{238}U$ reaction, $\langle I_z \rangle$ increases steadily with Q-value. Because of the high fission barriers for nuclei near Au, values of $\langle I_z \rangle$ were obtained only for the

most negative Q-values of the $^{40}Ar + ^{197}Au$ reaction. For both systems, $\langle I_z \rangle$ increases as Z_3 decreases, reflecting the rigid rotation partition of the exit channel angular momentum. Larger values of $\langle I_z \rangle$ are observed for reactions with the ^{197}Au target relative to those with the ^{238}U target. This difference reflects the strong bias towards fission from high-spin states of the gold-like nuclei introduced by their large fission barriers. The mass asymmetry dependence of the in-plane angular distributions is better discussed together with the rest of the data available in the literature, as is done in the next section.

5. Systematics of In-Plane Angular Distributions

An important quantity that can be obtained from the data is the difference between the in-plane variances of the TLF's spin distribution. Such a difference is only available from sequential fission angular distributions and is the central reason for the present study. At the same time it is interesting to compare the results of the present study with the previous data for the in-plane sequential fission angular distributions. The data should be placed on the same footing so that meaningful comparisons can be made. For example, in order to study the alignment of the intrinsic spin of the fissioning nucleus as a function of the mass asymmetry of the dinuclear complex, we need a series of reaction systems with the same total mass at the same temperature and total angular momentum. Since such data are not available, comparisons must be made after removing the effects of any quantity that is varying. A survey of the literature shows that extensive data are available in the range of 100 to 150 MeV energy loss for systems with total masses in the range of 217 to 328 amu. For this limited Q-value range the temperature of the dinuclear system varies slowly as a function of mass asymmetry and can be assumed to constant. In contrast, the average orbital angular momentum of the systems varies substantially with asymmetry and such a variation must be taken into account.

In addition, fitting Eqs. 4 and 5 to the FF angular distributions only determines the three parameters, q_2, q_3 and q_4. This leaves five unknowns (σ_x, σ_y, σ_z, $\langle I_z \rangle$, and K_0^2) and only three equations, Eq. 6, 8 and 9. One unknown variable can be removed by taking a value for K_0^2 from fission systematics and a second through an external assumption such as: forcing one of the σ's to be 0, as in reference 4; utilizing the prediction of the statistical equilibrium model that $\sigma_x = \sigma_z$; or assigning $\langle I_z \rangle$ an external value such as that predicted for rigid rotation of the system, as in reference 10. An alternative approach is to utilize the ratio q_3/q_2 which is equal to the in-plane anisotropy divided by the square of the aligned spin. From equations 6 and 8 one can write:

$$q_3 \,/\, q_2 = (\sigma_y^2 - \sigma_x^2) \,/\, 2 \langle I_z \rangle^2 \qquad 11.$$

The calculation of this ratio for the previous data [2-4,9,10]) is summarized in Table V, and its variation is shown in fig. 12A as a function of mass asymmetry, $(M_1 \,/\, M_1+M_2)$, of the DIC products. (The data were those for which the energy loss was as near to 150 MeV as possible.) The data in fig. 12A have a large scatter, due to their differing values of $\langle I_z \rangle$. In the rigid rotation limit, $\langle I_z \rangle$ is given by the ratio of the moment of inertia of the fissioning nucleus, $\mathcal{I}_{TLF}$, to the sum of the moments of inertia multiplied by the average-entrance-channel-orbital-angular momentum, L_{avg},:

$$\langle I_z \rangle_{RR} = \left(\frac{\mathcal{I}_{TLF}}{\mathcal{I}_{TLF} + \mathcal{I}_{PLF} + \mu R^2} \right) L_{avg} \qquad 12.$$

with $\mathcal{I}_{PLF}$ being the moment of inertia of the nonfissioning nucleus.

We have attempted to remove the variation of $\langle I_z \rangle$ in the observed values of q_3/q_2 by multiplying this quantity by two times the square of a

simple estimate of $\langle I_z \rangle_{RR}$. For this simple estimate we have used spherical moments of inertia and have taken L_{avg} to be 2/3 of L_{max}. We have also scaled the values of the moment of inertia of each dinuclear system to that of $^{40}Ar + ^{238}U$ system. Thus, a new quantity, δ^2, can be defined as:

$$\delta^2 = 2\left(\frac{q_3}{q_2}\right)\left\{\frac{278}{A_1+A_2}\right\}^{5/3}\left\{\left(\frac{\mathcal{J}_{TLF}}{\mathcal{J}_{TLF}+\mathcal{J}_{PLF}+\mu R^2}\right) L_{avg}\right\}^2 \qquad 13.$$

which should be approximately equal to the difference between the variances of the spin distribution along the two in-plane coordinates:

$$\delta = (\sigma_y^2 - \sigma_x^2)^{1/2} . \qquad 14.$$

The variation of δ is shown in fig. 12B as a function of mass asymmetry. This simple treatment has gone a long way towards systematizing the data in fig. 12A. The striking result of this treatment is that the strong oscillations of q_3/q_2 noted for several entrance channels has been removed. Overall, δ appears to increase when $M_1/(M_1+M_2)$ decreases indicating that σ_y becomes progressively larger than σ_x as the mass split becomes asymmetric. This trend is in qualitative agreement with the statistical equilibrium model.

The predictions of the statistical equilibrium model developed in references 11 and 12 can also be quantitatively tested with the systematic data presented in fig. 12B. This comparison is quite direct because the the model predicts values of σ_x^2 and σ_y^2 as a function of temperature and mass asymmetry of the dinuclear system. The predictions for two touching spheres, and a total mass of 278 amu at a temperature of 2.1 MeV are shown in fig. 12B. The model calculations for two touching spheres overestimate the misalignment along the symmetry axis throughout the mass asymmetry range. As was shown for the ^{20}Ne + Au and U systems,

this discrepancy is probably due to the neglect of either deformation or interfragment separation (neck formation) in the present model.

A first-order estimate of the effect of deformation on the model calculations can be made by allowing the target-like fragment to deform along the line-of-centers of the dinuclear system. Model calculations of δ for a sphere-spheroid system are also shown in fig 12B, labeled by the ratio of the axes of the spheroid (c/a). As the deformation increases, the tilting mode stiffens causing σ_y to decreas and thus δ to decrease. The calculations show that an axis ratio of 1.4 to 1.8 is needed to reproduce the dependence of the data on mass asymmetry. Slightly larger deformations of the TLF (c/a = 2) were necessary to reproduce average TKE values in the exit channel of the data from the present study (see appendix).

Conclusion

We have reported measurements of the angular distributions from sequential fission in the reaction of 340 MeV ^{40}Ar with ^{197}Au and ^{238}U. Sequential fission was observed over a broad range of energy losses with the uranium target and over a narrower range with the gold target. All the angular distributions were strongly focussed into the plane of the deep-inelastic collision. The in-plane angular distributions were isotropic at small negative Q-values but became anisotropic as the Q-value became more negative. The angular distributions were also measured as a function of the mass split in the initial DIC for both targets. The anisotropy of the in-plane angular distributions increased as the fragments became more symmetric for both reaction systems. The symmetry of the FF angular distributions indicated that the variances of the spin distributions along the Z axis and the Y axis were generally the same.

The data from the present study were combined with the previously reported sequential fission data (with energy losses in the neighborhood of 150 MeV). The in-plane anisotropy of the combined data was summarized as the ratio of the difference between the in-plane variances to the square of the aligned spin. The effect of the variation of $\langle I_z \rangle$ in the data set was approximately removed from the fitted parameter leaving a systematic variation of the difference between the in-plane variances of the fragment's spin distribution as a function of mass asymmetry. The variance along the line of centers of the dinuclear complex was found to be larger than that perpendicular to it. Qualitative agreement was obtained between the data and a simple statistical equilibrium model based on the degrees of freedom of two spheres in contact. More quantitative agreement with the data was obtained by allowing the heavier fragment to deform in the same model.

Appendix

In the present study, one axis (orthogonal to the quantization axis of the spin distribution which governs the FF angular distribution) was assumed to lie along the line-of-centers of the dinuclear complex at the scission point. A shift angle, Ψ, is defined as the amount of rotation necessary to bring this axis into alignment with the direction of the recoiling target nucleus in the laboratory. A value for Ψ was obtained for each angular distribution by tracing the path of the fragments in the exit channel back along a Coulomb trajectory to the point of contact. The Coulomb trajectory can be calculated with knowledge of: (1) the amount of orbital angular momentum in the exit channel, (2) the direction of rotation of the dinuclear complex, and (3) the point of contact of the two nuclei which depends, of course on the shapes of the nuclei.

The average value of the exit channel orbital angular momentum, $\langle L_f \rangle$, was estimated by conserving the total angular momentum:

$$\langle L_i \rangle = \langle L_f \rangle + \langle I_{PLF} \rangle + \langle I_Z \rangle \qquad \text{A-1.}$$

where $\langle L_i \rangle$ is the average initial orbital angular momentum for a given TKEL bin, $\langle I_{PLF} \rangle$ and $\langle I_Z \rangle$ are the average intrinsic spins of the projectile-like and target-like products, respectively. An average value of $\langle L_i \rangle$ was estimated in a sharp cutoff model by dividing the trapezoidal L distribution between L_{crit} and L_{max} in proportion to the cross section. The values of L_{crit} for the different targets were taken to be 143 ħ and 124 ħ from the measurements of Rivet et al. [25]) and Kildir et al. [26]) for the reactions of ^{40}Ar with ^{197}Au and ^{238}U, respectively.

The intrinsic spins of the reaction products can be estimated using two different methods. From equations 4 and 5, the out-of-plane angular distribution can be written:

$$\left(\frac{W(\Theta^H,\Phi^H)}{W(90,\Phi^H)}\right) = \left(\frac{R(90,\Phi^H)}{R(\Theta^H,\Phi^H)}\right) e^{-\left(\frac{q_2}{2}\right)\left\{\frac{\cos^2\Theta^H}{R^2(\Theta^H,\Phi^H)} - \frac{1}{R^2(90,\Phi^H)}\right\}} \qquad \text{A-2}$$

The angle $\Theta_{1/2}$ at which $W(\Theta^H,\Phi^H)$ is half its in-plane value can be related to the spin as follows. Consider equation A-2 when the in-plane angle is equal to $\Psi \pm 45°$ and at the half-angle, $\Theta^1/_2$:

$$\ln\left(\frac{2}{R(\Theta^1/_2)}\right) = \left(\frac{q_2}{2}\right)\left(\frac{\cos^2\Theta^1/_2}{R^2(\Theta^1/_2)}\right) \qquad \text{A-3.}$$

where $R^2(\Theta^1/_2) = 1 + q_4 \cos^2 \Theta^1/_2$. This makes q_2 equal to a simple function of the half-angle:

$$q_2 = \left(\frac{R^2(\Theta^1/_2)}{\cos^2 \Theta^1/_2}\right) \ln\left(\frac{4}{R^2(\Theta^1/_2)}\right) \qquad \text{A-4.}$$

Note that in many cases q_4, which is proportional to the difference between σ_z^2 and the average of σ_x^2 and σ_y^2, is small compared to 1 so that:

$$q_2 = \ln 4 \ / \cos^2 \Theta^1/_2 \qquad \text{A-5.}$$

The second method of estimating the spin of the fissioning nucleus utilizes the fitted values of q_2 (Eq. 6). Values of K^2_{eff} were determined taking σ_x and σ_y from the equilibrium statistical model [11,12]) and values for K_0^2 by scaling the empirical expression of Puigh et al. [4]). For this estimate, K_0^2 of uranium was scaled by the ratio of the effective moments of inertia from Cohen and Swiatecki [27]):

$$K_0^2(x) = [\mathcal{J}_{eff}(x) / \mathcal{J}_{eff}(U)] \, 19.37 \, (E_f)^{1/2} \qquad \text{A-6.}$$

where E_f is the energy available above the saddle point.

The first estimate of $\langle I_Z \rangle$ made from the half-angles of the out-of-plane angular distributions with equation A-4 was used to calculate Ψ. A new value of q_2 was obtained from a fit to the angular distribution using the calculated value of Ψ. This new value of q_2 was generally within 10 percent of the original estimate. A second estimate of $\langle I_Z \rangle$ and then of Ψ was made and the angular distributions were refitted. The calculations and final results for $\langle I_Z \rangle$ are summarized in Table IV.

The final quantity needed to calculate L_f in equation A-1 is $\langle I_{PLF} \rangle$. The spin of the light fragment was calculated from that of the heavy fragment with the statistical equilibrium prediction that the ratio of the spins should equal that of the moments of inertia:

$$\mathcal{J}_{TLF} / \mathcal{J}_{PLF} = (A_{TLF} / A_{PLF})^{5/3}. \qquad \text{A-7.}$$

The ratios are large, 14.3 for argon plus gold and 19.5 for argon plus uranium, forcing the spin of the PLF to be on the order of 2 or 3$\hbar$.

With a value for the exit channel orbital angular momentum from Eq. A-1, the Coulomb trajectory can be retraced back to the scission configuration. So the shift angle depends on the extension of the dinuclear system and thus on the shapes of the nuclei. The nuclei that emerge from DIC are known to be strongly deformed [28]), and the effect of this deformation on the direction of the line-of-centers should not be

ignored. A measure of the shapes of the nuclei can be found in the TKE distributions. The measured values of the inclusive TKE as a function of PLF Z_3 for the reaction of ^{40}Ar with ^{197}Au are shown in fig. 13 along with values calculated for two shape configurations. These TKE values were calculated for a rigidly rotating dinuclear complex at its equilibrium spheroidal shape[29]). The two spheroidal shape configurations with equal prolate deformation of both fragments (a ratio of axes, c/a = 1.9), lower full curve, and prolate deformation of only the heavy fragment (c/a = 2.), upper full curve. The data points are generally consistent with the latter description of the shape of the fragments. This latter sphere-spheroid configuration was taken to be the scission configuration. We estimate the uncertainty in the endpoint of the Coulomb trajectory to be about 1 fm. The effects of such an uncertainty on the fitting process are discussed in the text.

This work was supported, in part, by the Director, Office of Energy Research, Division of Nuclear Physics of the Office of High Energy and Nuclear Physics of the U.S. Department of Energy under contract DE-AC03-76SF00098, and by the National Science Foundation under Grant No. PHY 80-17605.

* Permanent address: Department of Chemistry, Washington University, Saint Louis, MO 63130

+ Permanent address: Comisiòn Nacional de Energìa Atòmica, Buenos Aires, Argentina

References

1. V.M. Strutinski, Nucl. Phys. 27 (1961) 348.

2. P. Dyer, R.J. Puigh, R. Vandenbosch, T.D. Thomas, M.S. Zisman, and L. Nunnelley, Nucl. Phys. A322 (1979) 205.

3. D.v. Harrach, P. Glässel, Y. Civelekoglu, R. Männer, and H.J. Specht, Phys. Rev. Lett. 42 (1979) 1728.

4. R.J. Puigh, P. Dyer, R. Vandenbosch, T.D. Thomas, L. Nunnelley, and M.S. Zisman, Phys. Lett. 86B (1979) 24.

5. e.g., L.G. Sobotka, R.J. McDonald, G.J. Wozniak, D.J. Morrissey, A.J. Pacheco, and L.G. Moretto, Phys. Rev. C21 (1983) 219, and references therein

6. e.g., A.J. Pacheco, G.J. Wozniak, R.J. McDonald, C.C. Hsu, L.G. Moretto, D.J. Morrissey, L.G. Sobotka, and F.S. Stephens, Nucl. Phys. A397 (1983) 313, and references therein, and A. Lazzarini, V. Metag, A.G. Seamster, R. Vandenbosch, and R. Loveman, Phys.

Rev. Lett. 46 (1981) 988.

7. e.g., R.J. Puigh, H. Doubre, A. Lazzarini, A. Seamster, R. Vandenbosch, M.S. Zisman, and T.D. Thomas, Nucl. Phys. A336 (1980) 279, and G. Mouchaty, D.R. Haenni, S. Nath, U. Garg, and R.P. Schmitt, Z. Phys. A316 (1984) 285.

8. W. Dünnweber, W. Hering, H. Puchta, R. Ritzka, W. Trautmann, W. Trombik and C. Egelhaaf, Phys. Rev. Lett. 52 (1984) 1405.

9. D.J. Morrissey, G.J. Wozniak, L.G. Sobotka, A.J. Pacheco, R.J. McDonald, C.C. Hsu, and L.G. Moretto, Nucl. Phys. A389 (1982) 120.

10. C. Le Brun, J.F. Lecolley, F. Lefebvres, M. L'Haridon, A. Osmont, J.P. Patry, J.C. Steckmeyer, and R. Chechik, Phys. Rev. C25 (1982) 3212. and J.C. Steckmeyer, et al. Nucl. Phys A, submitted for publication, 1984.

11. L.G. Moretto and R.P. Schmitt, Phys. Rev. C21 (1980) 204.

12. R.P. Schmitt and A.J. Pacheco, Nucl. Phys. A379 (1982) 313.

13. R.A. Broglia, G. Pollarolo, C.H. Dasso, and T. Døssing, Phys. Rev. Lett. 43 (1979) 1649.

14. R. Vandenbosch, Phys. Rev. C20 (1979) 171.

15. G. Wolschin, Nucl. Phys. A316 (1979) 146.

16. J. Randrup, Nucl. Phys. A383 (1982) 468.

17. M.M. Fowler and R.C. Jared, Nucl. Instr. and Meth. 124 (1975) 342.

18. G.U. Rattazzi, R.P. Schmitt, G.J. Wozniak, and L.G. Moretto, Lawrence Berkeley Laboratory Report LBL-9711, 1980 (unpublished), p.130.

19. J.B. Moulton, J.E. Stephenson, R.P. Schmitt, and G.J. Wozniak, Nucl. Instr. and Meth. 157 (1978) 325.

20. V.E. Viola, Jr., Nucl. Data A1 (1966) 391.

21. B.B. Back and S. Bjørnholm, Nucl. Phys. A302 (1978) 343.

22. T. Døssing, Nucl. Phys. A357 (1981) 488.

23. L.G. Moretto, S.K. Blau, and A.J. Pacheco, Nucl. Phys. A364 (1981) 125.

24. D.v. Harrach, Private communication.

25. M.F. Rivet, D. Logan, J.M. Alexander, D. Gerreau, E. Duek, M.S. Zisman, and M. Kaplan, Phys. Rev. C25 (1982) 2340.

26. M. Kildir, D. Logan, M. Kaplan, M.S. Zisman, D. Guerreau, J.M. Alexander, and L.C. Vaz, Z. Phys. A306 (1982) 323.

27. S. Cohen and W.J. Swiatecki, Ann. Phys. (N.Y.) 22 (1963) 406

28. G. Wolschin, Phys. Lett. 88B (1979) 35, and C. Riedel and G. Wolschin, Z. Phys. A294 (1980) 17.

29. L.G. Moretto and L.G. Sobotka, Z. Phys. A303 (1982) 299.

TABLE I Results of the angular distribution fitting

Target	TKEL (MeV)	Z_3	Ψ (deg.)	q_2	q_3	q_4	χ_ν^2
^{238}U	0- 40	9-27	38*	2.0 (.1)	.00(.09)	.05(.11)	1.6
	41- 90	9-27	45*	3.6 (.1)	.00(.09)	.12(.06)	1.1
	91-140	9-27	65	4.8 (.1)	.29(.07)	.22(.06)	1.5
	141-190	9-27	74	5.6 (.2)	.35(.09)	.14(.12)	1.6
	91-190	9-27	71	5.0 (.1)	.33(.10)	.05(.03)	1.2
	91-190	9-16	74	5.6 (.1)	.19(.09)	.20(.05)	1.1
	91-190	17-18	71	4.4 (.2)	.28(.10)	-.20(.06)	1.8
	91-190	19-27	63	3.3 (.2)	.35(.15)	-.45(.04)	1.8
^{197}Au	91-190	9-27	69	10.7 (.2)	.48(.07)	.51(.04)	1.4
	91-190	9-16	72	12.7 (.3)	.30(.07)	.72(.07)	1.4
	91-190	17-18	69	11.2 (.5)	.52(.13)	.68(.12)	1.2
	91-190	19-27	62	7.6 (.1)	.65(.06)	.02(.05)	2.1

NOTES

* arbitrary because the data is isotropic in-plane as indicated by the zero value of q_3.

TABLE II Results of constrained angular distribution fitting*

Target	TKEL (MeV)	Z_3	Ψ (deg.)	q_2	q_3^*	χ_ν^2
^{238}U	0- 40	9-27	38	2.0 (.1)	.01(.06)	1.5
	41- 90	9-27	45	3.4 (.1)	.03(.04)	1.0
	91-140	9-27	65	4.7 (.2)	.27(.03)	1.4
	141-190	9-27	74	4.7 (.2)	.19(.05)	1.9
	91-190	9-27	71	4.5 (.1)	.11(.03)	1.5
	91-190	9-16	74	4.9 (.1)	.00(.04)	1.3
	91-190	17-18	71	4.5 (.2)	.17(.05)	2.2
	91-190	19-27	63	3.2 (.2)	.29(.05)	1.5
^{197}Au	91-190	9-27	69	7.8 (.2)	.00(.03)	3.9
	91-190	9-16	72	9.3 (.3)	.04(.05)	3.1
	91-190	17-18	69	8.5 (.5)	.28(.10)	2.6
	91-190	19-27	62	6.1 (.2)	.32(.04)	3.5

NOTES

* The values of q_3 and q_4 were forced to be equal and opposite in sign.

TABLE III Results of constrained angular distribution fitting*

Target	TKEL (MeV)	Z_3	Ψ (deg.)	q_2	q_3^*	χ_ν^2
^{238}U	0- 40	9-27	38	2.0 (.1)	.00(.07)	1.5
	41- 90	9-27	45	3.4 (.1)	.03(.04)	1.0
	91-140	9-27	65	6.0 (.2)	.27(.08)	1.6
	141-190	9-27	74	6.0 (.2)	.32(.07)	1.9
	91-190	9-27	71	5.5 (.1)	.22(.03)	1.3
	91-190	9-16	74	5.5 (.1)	.19(.04)	1.1
	91-190	17-18	71	5.3 (.2)	.20(.07)	2.0
	91-190	19-27	63	4.7 (.2)	.32(.09)	1.7
^{197}Au	91-190	9-27	69	10.6 (.2)	.49(.04)	1.4
	91-190	9-16	72	11.5 (.3)	.41(.05)	1.5
	91-190	17-18	69	11.4 (.5)	.56(.10)	1.3
	91-190	19-27	62	10.0 (.3)	.55(.05)	2.8

NOTES

* The values of q_3 and q_4 were forced to be positive and equal.

TABLE IV Estimate of the Fragment Spins

Target	TKEL (MeV)	Z_3	$\Theta_{1/2}$ (deg.)	K_0^2 * (†)	σ_y^2 (†)	σ_x^2 (†)	K_{eff}^2 (†)	q_2^+	$\langle I_z \rangle^+$ ($\hbar$)
^{238}U	0- 40	9-27	36(4)	44	163	36	143	2.0	17 (1)
	41- 90	9-27	50(4)	132	353	78	348	3.6	35 (1)
	91-140	9-27	59(3)	185	489	108	483	4.8	48 (1)
	141-190	9-27	61(3)	225	597	132	590	5.6	58 (1)
	91-190	9-27	60(3)	166	516	114	481	5.0	49 (1)
	91-190	9-16	60(3)	269	543	120	601	5.6	58 (1)
	91-190	17-18	59(3)	166	516	114	481	4.4	46 (1)
	91-190	19-27	56(3)	144	461	102	426	3.3	38 (2)
^{197}Au	91-190	9-27	70(3)	120	393	107	370	10.7	63 (2)
	91-190	9-16	71(3)	154	428	117	427	12.7	74 (2)
	91-190	17-18	72(3)	120	393	107	370	11.2	64 (2)
	91-190	19-27	67(3)	105	375	103	344	7.6	51 (1)

NOTES

* Calculated at the cross section weighted average Q-value.

\+ All the initial estimates (except for one) made with the half-angle and Eq. (A-4) were within ten percent of the final fitted values reported here, see text.

† Units of $\hbar^2$

TABLE V Synopsis of the analysis of published data

System	<Q-value> (MeV)	Z_3	data type*	q_3/q_2	δ ($\hbar$)	reference
$^{20}Ne+^{197}Au$	-125	6-14	F	0.10 (.01)	16(1)	9
$^{20}Ne+^{238}U$	-125	6-14	F	0.11 (.02)	20(2)	9
$^{40}Ar+^{209}Bi$	-80	13	S	0.051(.01)	9(1)	10
	-80	14	S	0.055(.01)	9(1)	10
	-80	15	S	0.057(.01)	8(1)	10
	-80	16	S	0.063(.01)	8(1)	10
	-80	17	S	0.079(.01)	9(1)	10
$^{58}Ni+^{208}Pb$	-150+	all	A	0.02 (.04)	$5(^{+4}_{-5})$	3
	-150+	all	S	0.04 (.01)	7(1)	10
$^{58}Ni+^{238}U$	-80	all	A	0.03 (.06)	$7(^{+5}_{-7})$	3
$^{90}Zr+^{208}Pb$	-180+	all	A	0.01 (.02)	$4(^{+3}_{-4})$	3
$^{90}Zr+^{238}U$	-100	all	A	0.04 (.06)	$9(^{+5}_{-9})$	3
$^{86}Kr+^{209}Bi$	-154	32	A	0.03 (.01)	7(1)	2
	-154	35	A	0.05 (.02)	8(1)	2
	-154	38	A	0.04 (.01)	6(1)	2
$^{86}Kr+^{238}U$	-165	all	A	0.08 (.01)	16(1)	4

NOTES

* The ratio of q_3/q_2 was calculated in three ways depending on the type of data available: the angular distributions were Fitted, (F), to the data points, or published values of Gaussian Sigmas, (S), were used, or the value was calculated from the Anisotropy, (A), of an in-plane angular distribution and from the half-angle of the out-of-plane angular distribution.

+ The published data were integrated over Q-value, however the fission barriers of the Pb-like nuclei created an effective Q-value range for sequential fission.

Figure captions

1. Typical energy spectra of fission fragments are shown in the rest frame of the recoiling uranium-like nucleus for a constant in-plane laboratory angle (Φ^L=130°) and different out-of-plane angles (Θ^L) of the fission fragment. The loss of Gaussian shape with decreasing Θ is discussed in the text. [msux-83-475]

2. Contours of the coincidence cross section for detecting a sequential fission fragment are shown as a function of projectile-like fragment charge, Z_3 and total kinetic energy (TKE) for gold, (A), and uranium, (B), targets. Random coincidences are seen in part (A) at the highest probability for quasielastic events. [msux-82-292]

3. The probability of sequential fission as a function of the projectile-like fragment charge is shown for the two reaction systems. The abrupt dip at Z_3= 10 is most likely due to contamination of the singles cross sections by reactions on light elements (i.e. the Al backing for U). In general, the fission probability for reactions on Au is lower than that for U. The pronounced dip at Z_3 = 18 is due to the large contribution from quasielastic reactions whose product nuclei are at low excitation energies. [msux-82-296]

4. The probability of sequential fission is shown as a function of total kinetic energy (TKE). For both the U and Au data, the fission probalilities rise rapidly with decreasing TKE and saturate near unity. For the Au data, the onset of both the rise and saturation is shifted to smaller values of TKE by the larger fission barriers. The fall-off in fission probability below 200 MeV with the uranium target is due to contamination of the singles cross sections with reactions on the target backing.
[msux-82-300]

5. The out-of-plane angular distributions of sequential fission fragments from reactions with uranium are shown as a function of reaction Q-value. The data have been integrated over projectile-like fragment charge in the range of 9 to 27. The circles correspond to an in-plane angle of approximately 120° and the triangles to approximately 20° in the rest frame of the fissioning nucleus. The curves represent the fitted function discussed in the text. [msux-82-302]

6. The out-of-plane angular distributions from reactions with uranium are shown for different values of projectile-like fragment charge. The data fall in the TKE range of 150 to 250 MeV. The circles correspond to an in-plane angle of approximately 30° and the squares to approximately 120° in the rest frame of the fissioning nucleus. [msux-83-175]

7. The out-of-plane angular distributions from reactions with gold are shown for different values of projectile-like fragment charge. The data fall in the TKE range of 150 to 250 MeV. The circles correspond to an

in-plane angle of approximately 30° and the squares at approximately 120° in the rest frame of the fissioning nucleus. [msux-83-174]

8. The in-plane angular distribution of sequential fission fragments from reactions with uranium are shown for the same Q-value bins used in Figure 5. The curves represent the fitted function discussed in the text. The tick marks (|) indicate the symmetry point of the distributions, see text. [msux-83-171]

9. The in-plane angular distribution of sequential fission fragments from reactions with uranium for the same projectile-like fragment charge gates used in Figure 6 are shown. [msux-83-173]

10. The in-plane sequential fission angular distributions from the reaction with the gold target are shown. The four data sets were generated by gating on projectile-like fragment charge as in Figure 7. [msux-82-294]

11. The calculated value of the shift angle, ψ, as a function of Total Kinetic Energy Loss (TKEL) appears in (A). The variation of the fitted parameters from reactions with uranium is shown in parts (B), (C), and (D), see text. The filled squares represent the TKEL gated data, open symbols represent the Z_3 gated data with, circles 9-16, triangles 17-18, and squares 19-27. [msux-84-148]

12. (A) A measure of the in-plane anisotropy q_3/q_2 is shown as a function of the mass asymmetry of the reaction products. (B) The variation of $\langle I_z \rangle$ and the total mass of the system has been approximately removed from the in-plane anisotropies shown above as discussed in the text. The curves are statistical equilibrium model calculations for differing ratios, (c/a), of the major to minor axes of a spheroidal TLF, see text. [msu-84-464]

13. The calculated values of the centroids, (curves) of the TKE from separating deep-inelastic products are shown as a function of light fragment charge for two different shape configurations, see text. The values obtained from gaussian fits to the deep-inelastic peaks for each PLF Z are shown by the data points. Error bars indicate ± 1 sigma. The thin lines indicate a statistical model estimate of the effect on the TKE distributions [29]) of including a thermal width. [msux-83-399]

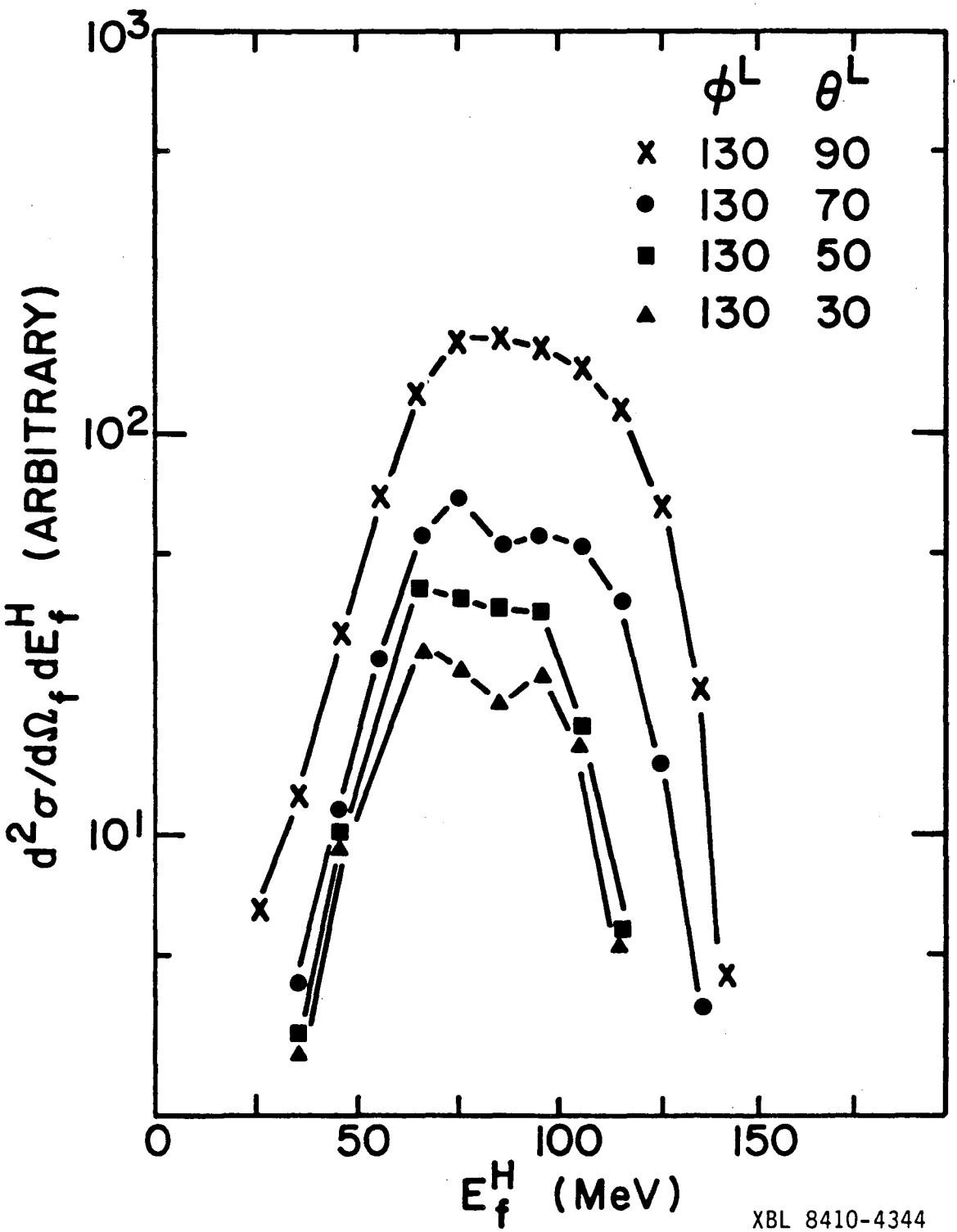

XBL 8410-4344

Fig. 1

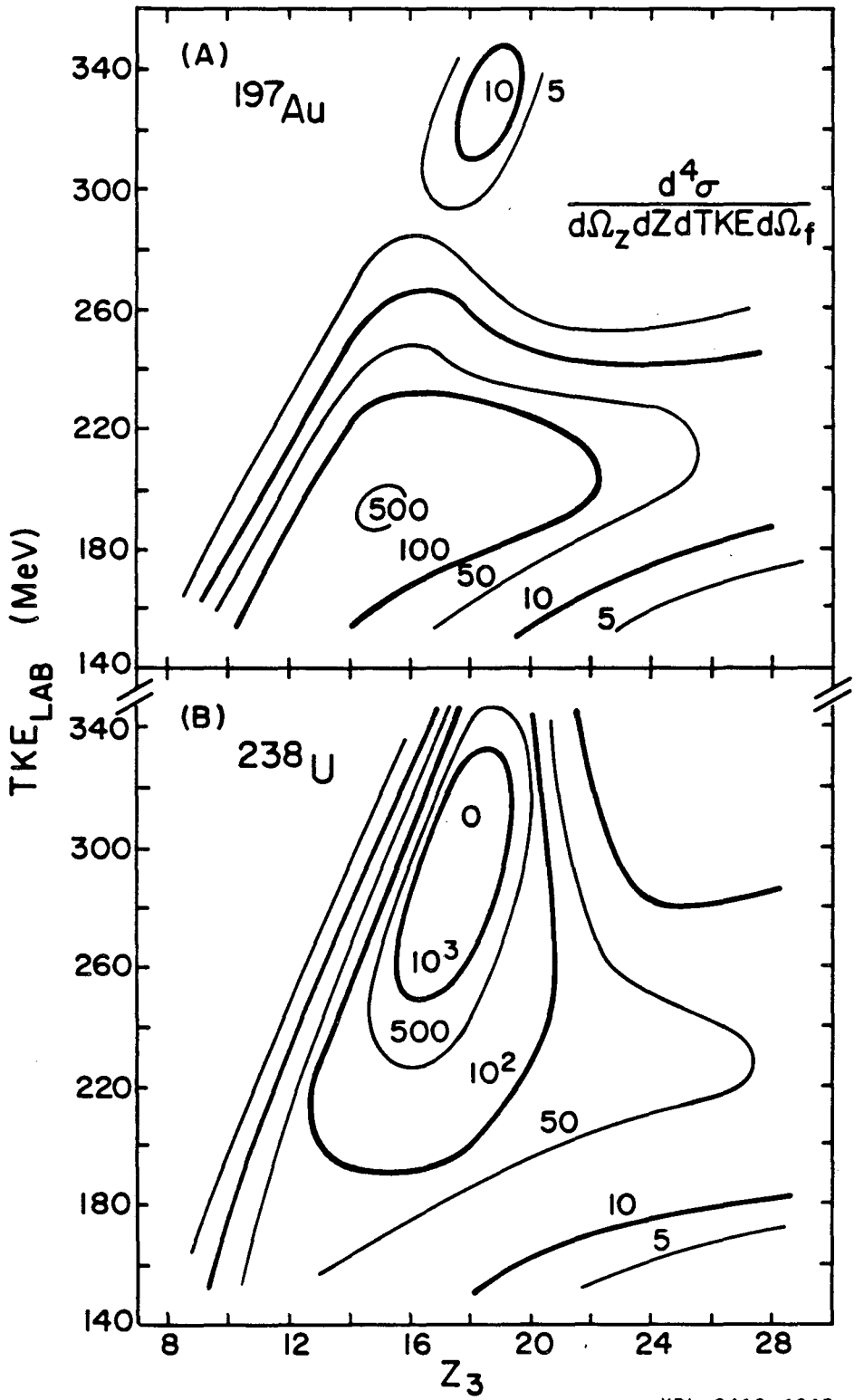

Fig. 2

XBL 8410-4345

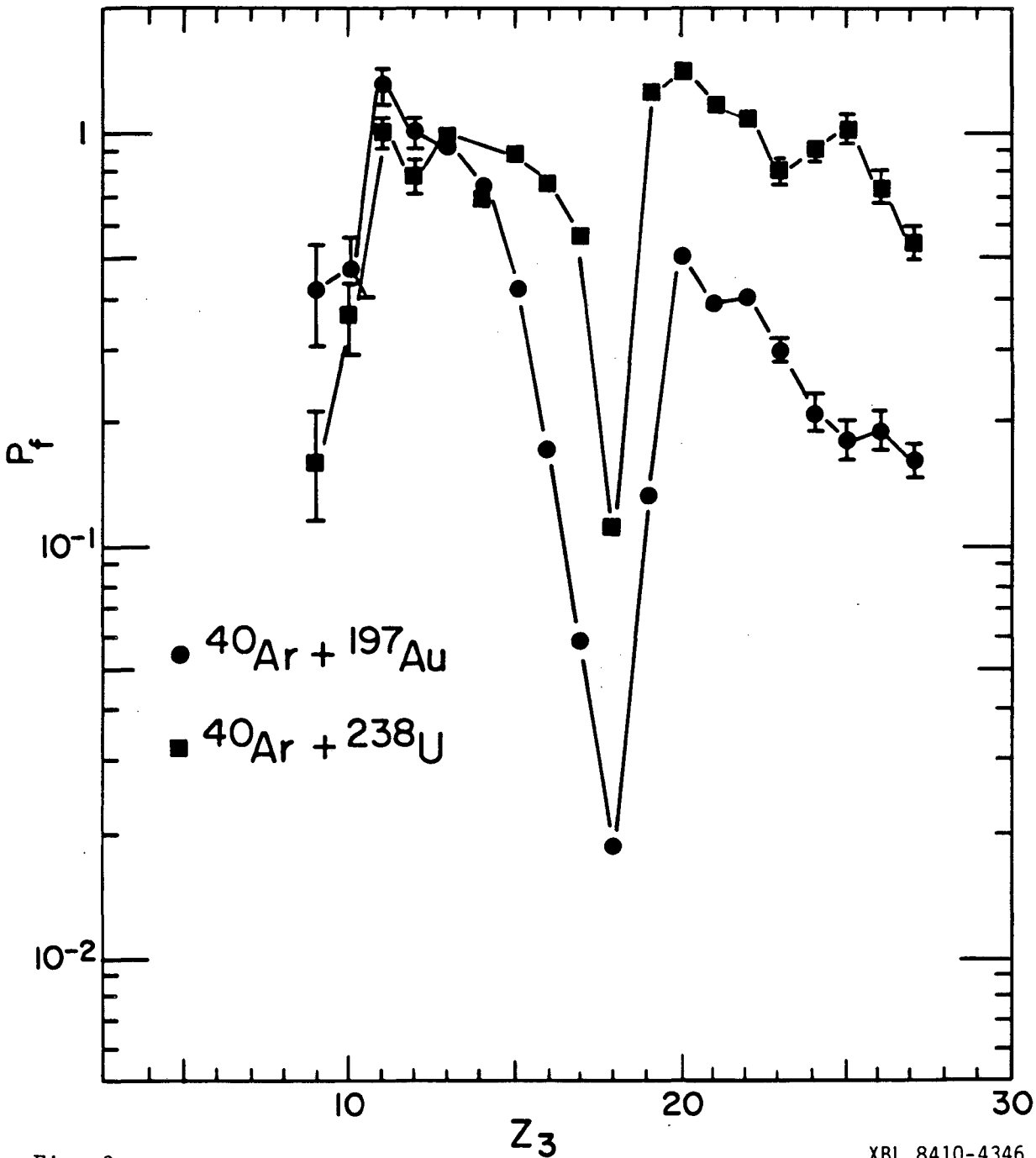

Fig. 3

XBL 8410-4346

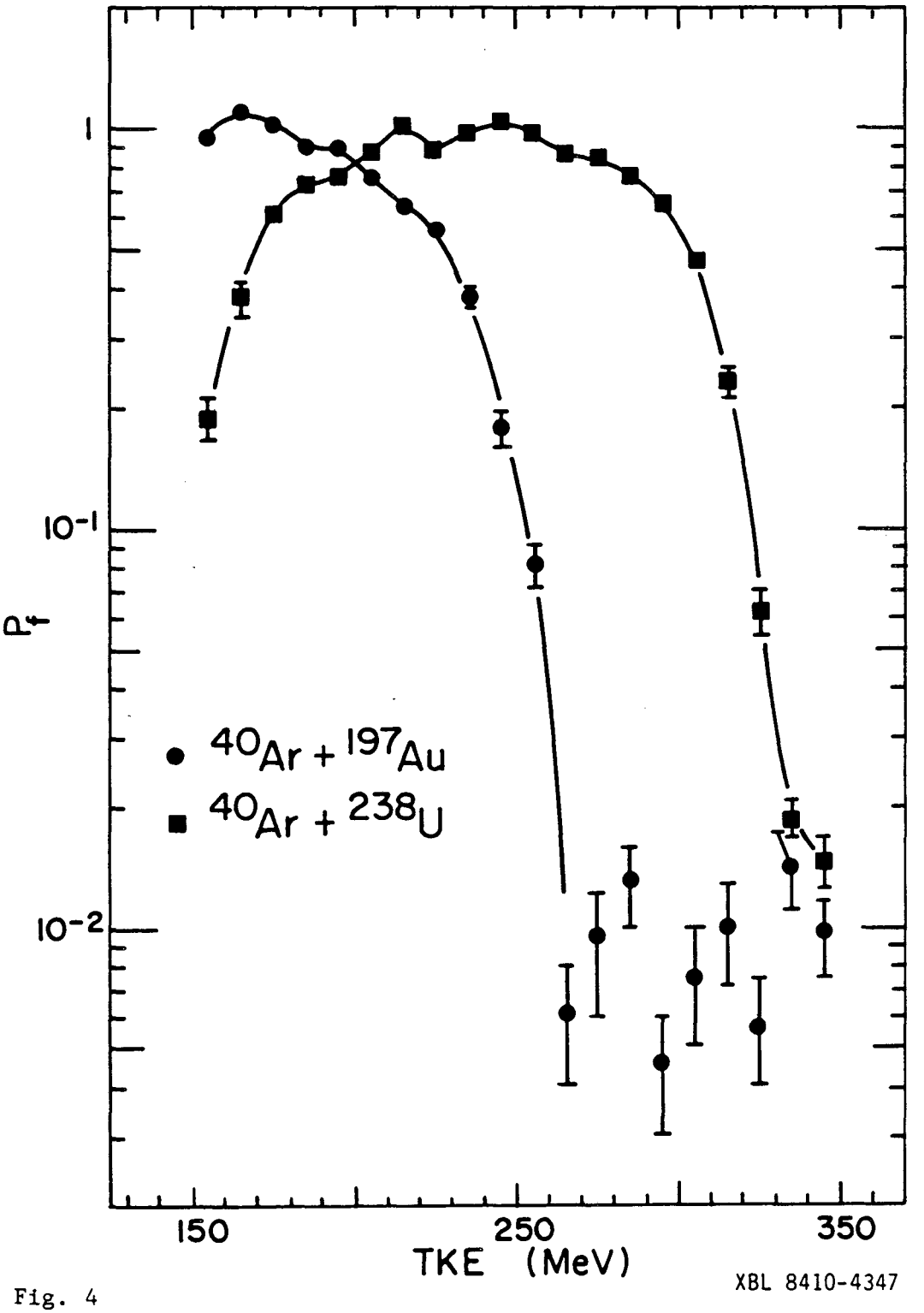

XBL 8410-4347

Fig. 4

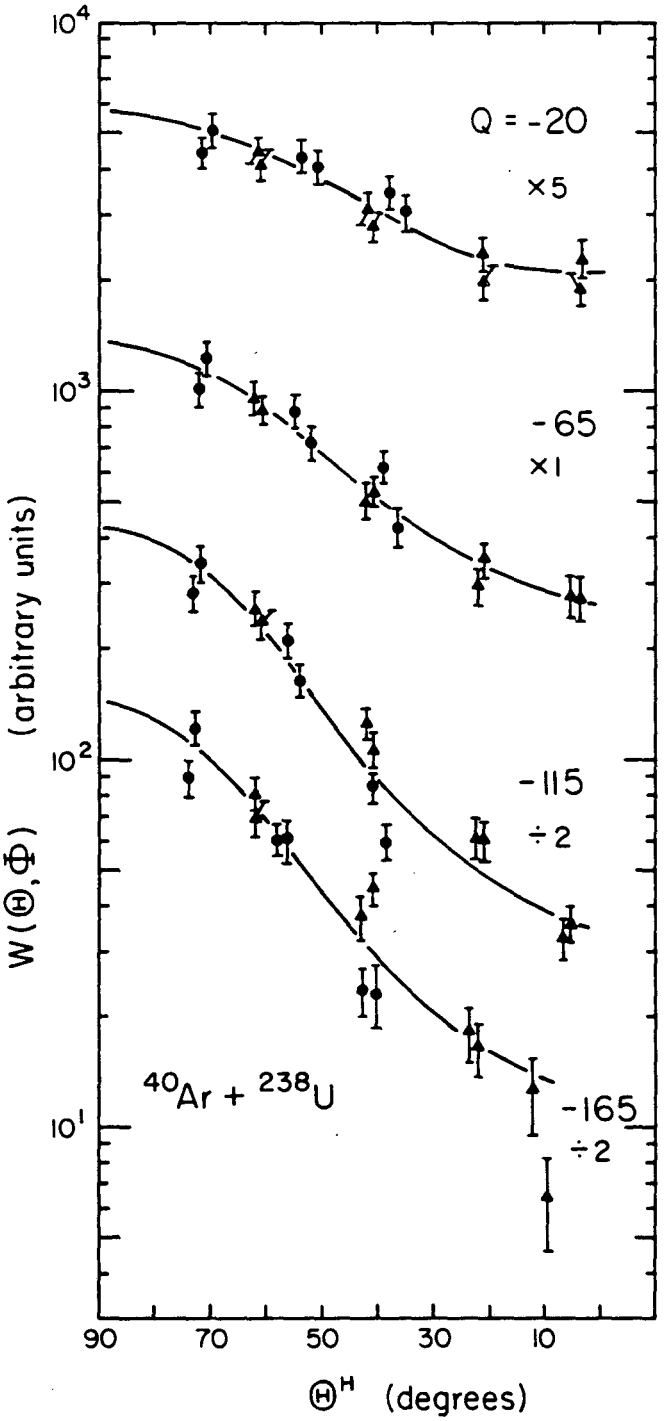

Fig. 5

XBL 8410-4348

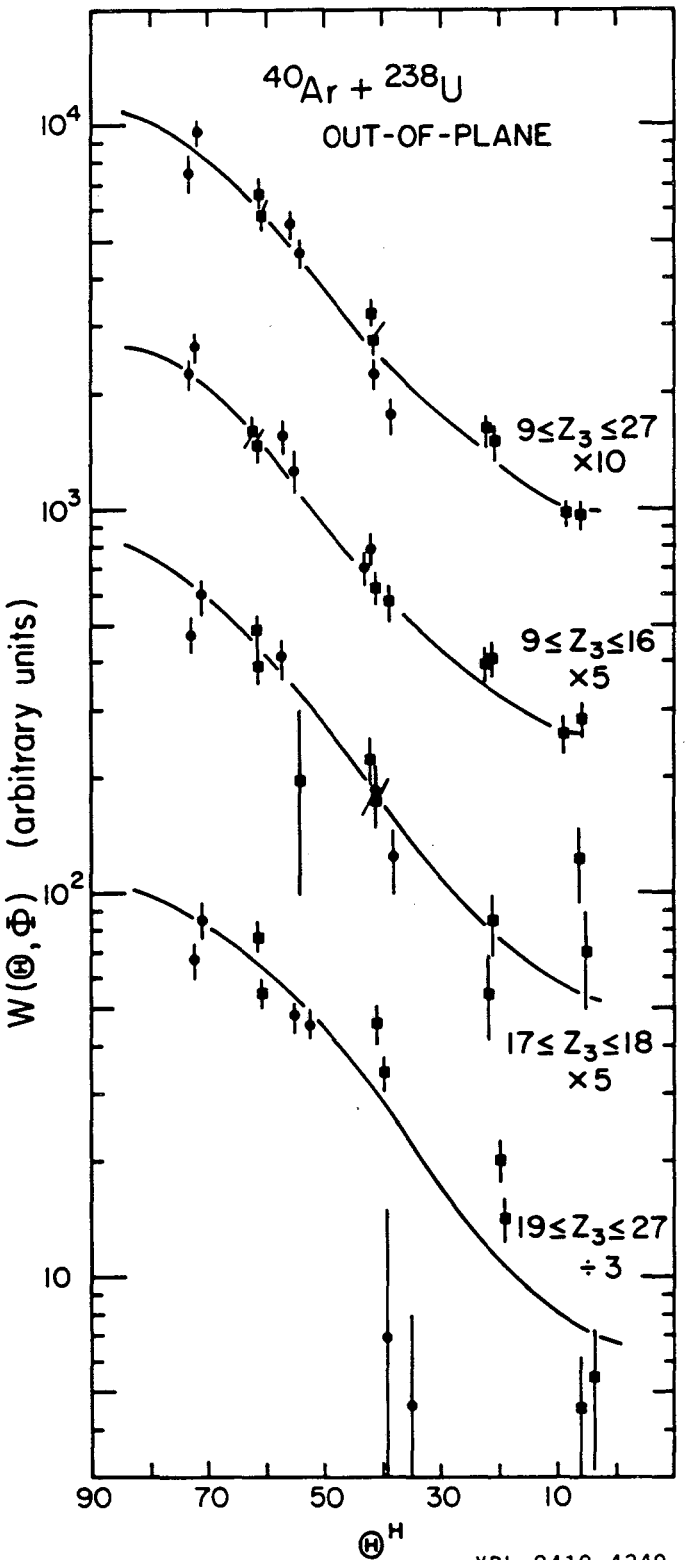

Fig. 6

XBL 8410-4349

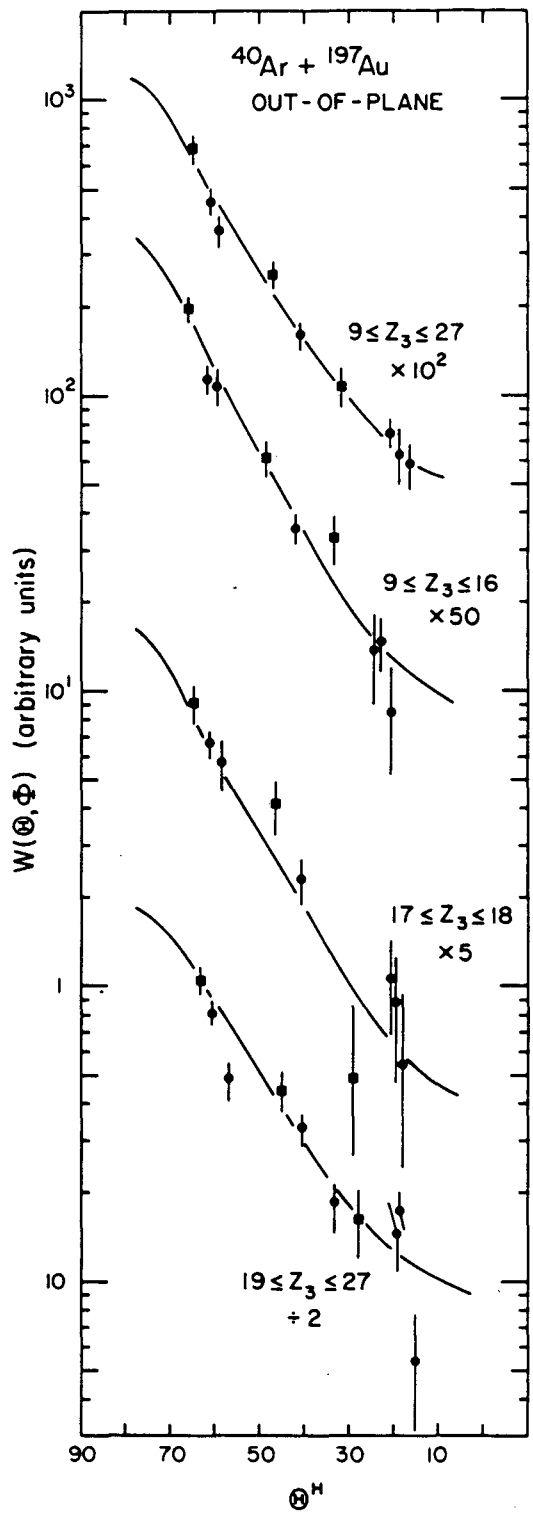

Fig. 7 XBL 8410-4350

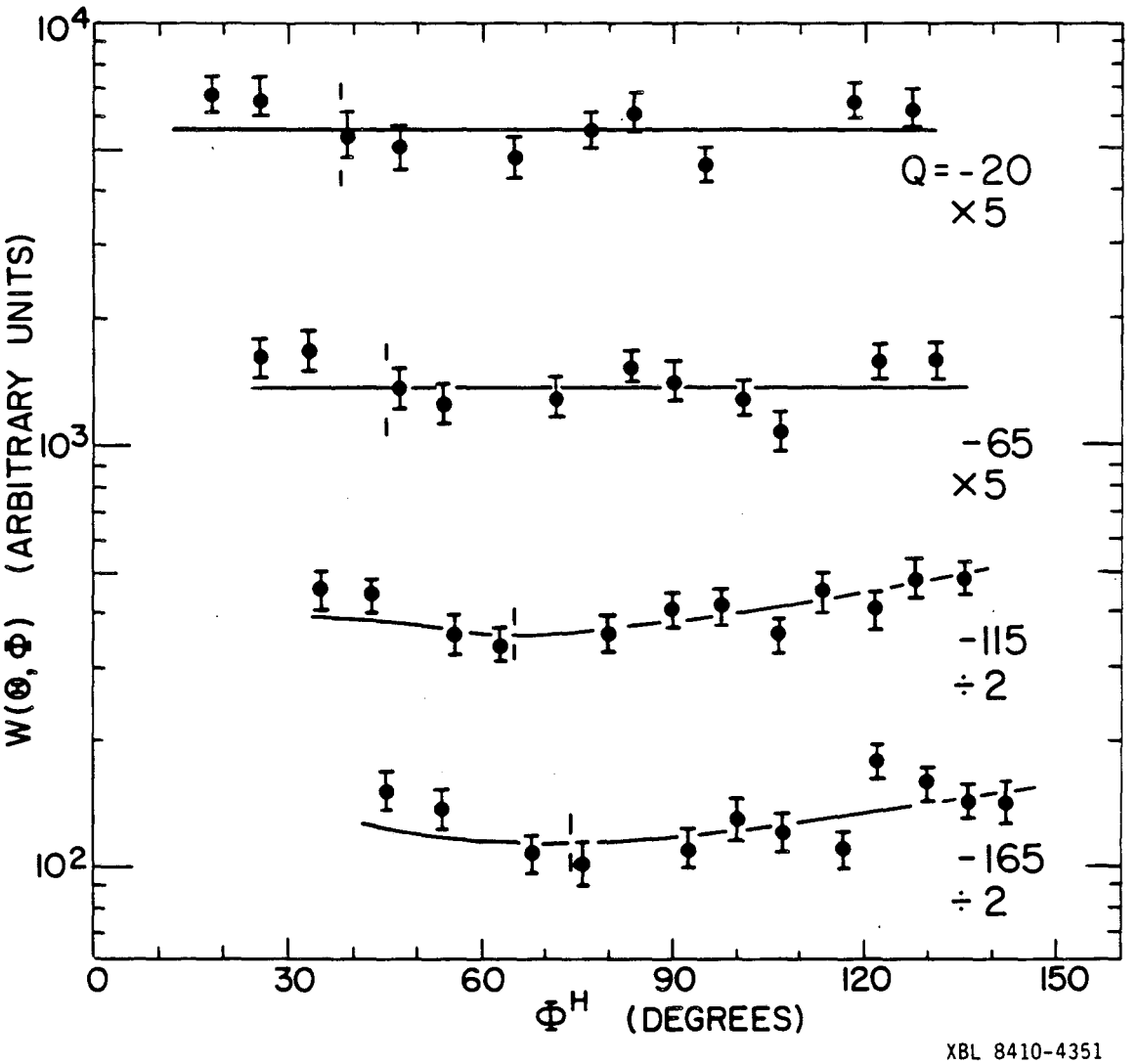
10^4
10^3
10^2
W(Θ, Φ) (ARBITRARY UNITS)
Q = -20
×5
-65
×5
-115
÷2
-165
÷2
0
30
60
90
120
150
Φ^H (DEGREES)
XBL 8410-4351

Fig. 8

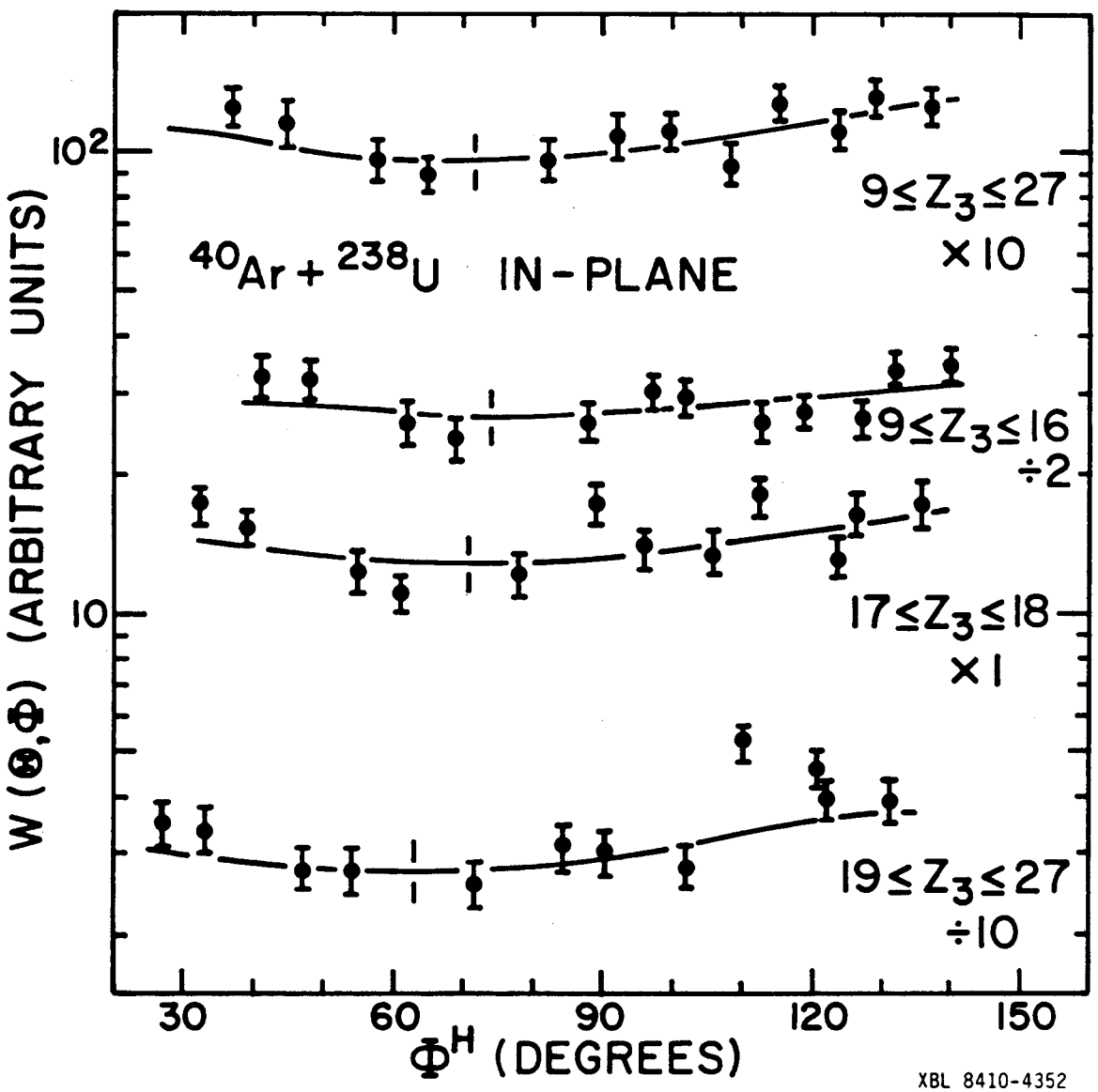
10^2
10
W (Θ,Φ) (ARBITRARY UNITS)
$^{40}Ar + ^{238}U$ IN-PLANE
$9 \le Z_3 \le 27$
×10
$9 \le Z_3 \le 16$
÷2
$17 \le Z_3 \le 18$
×1
$19 \le Z_3 \le 27$
÷10
30
60
90
120
150
Φ^H (DEGREES)
XBL 8410-4352

Fig. 9

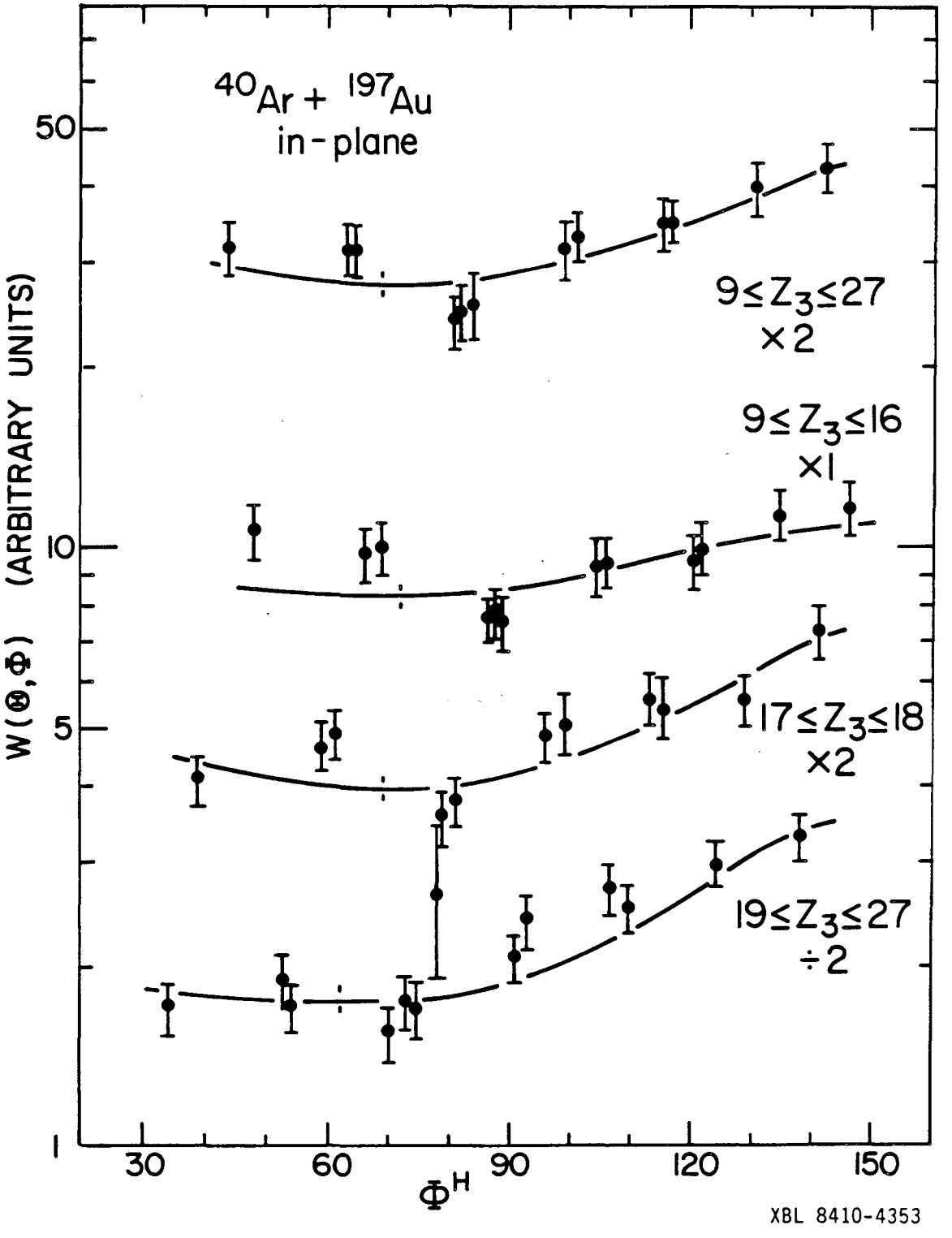
$^{40}Ar + ^{197}Au$
in-plane
$9 \leq Z_3 \leq 27$
×2
$9 \leq Z_3 \leq 16$
×1
$17 \leq Z_3 \leq 18$
×2
$19 \leq Z_3 \leq 27$
÷2
W(Θ,Φ) (ARBITRARY UNITS)
50
10
5
1
30
60
90
120
150
Φ^H
XBL 8410-4353

Fig. 10

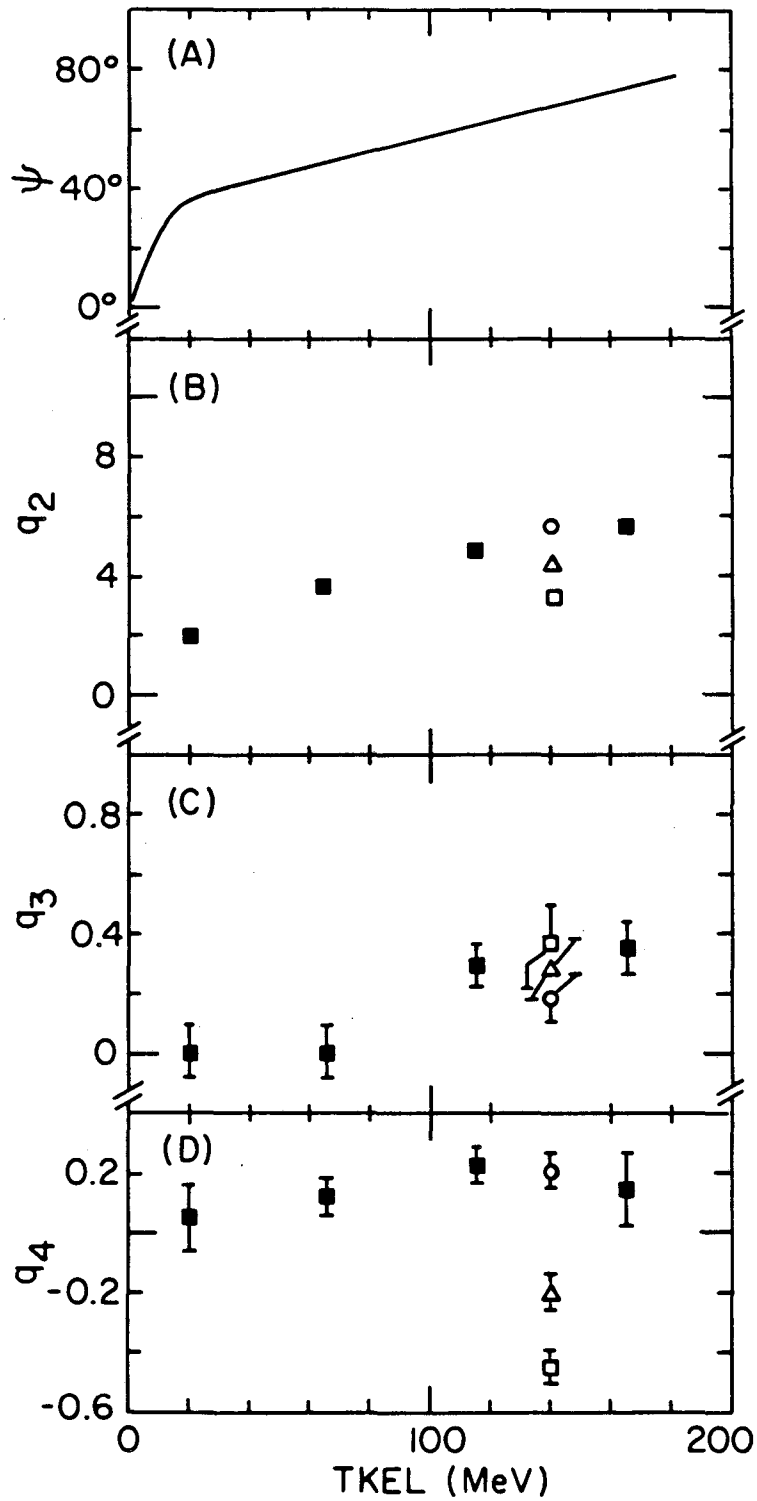

XBL 8410-4354

Fig. 11

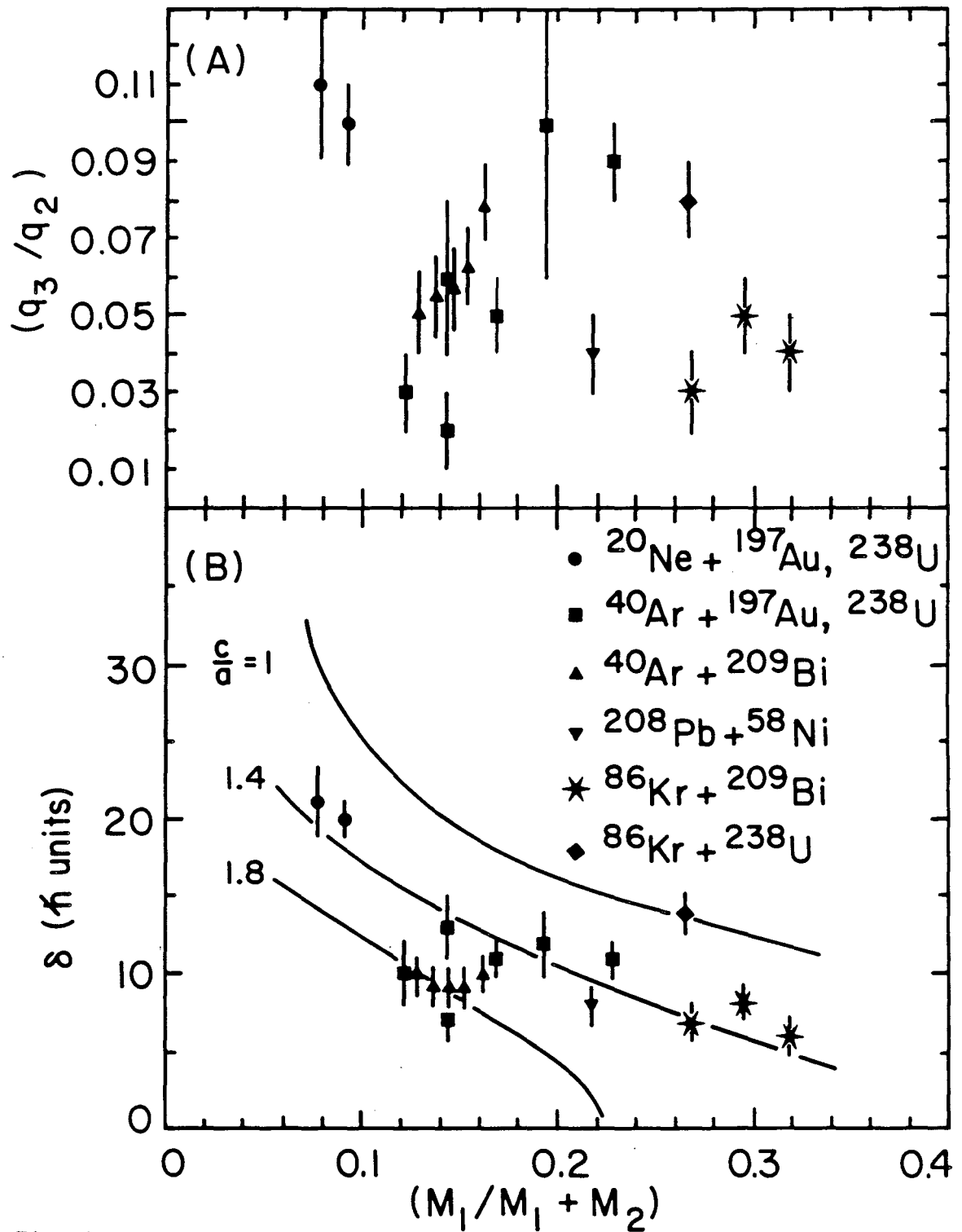

Fig. 12

XBL 8410-4343

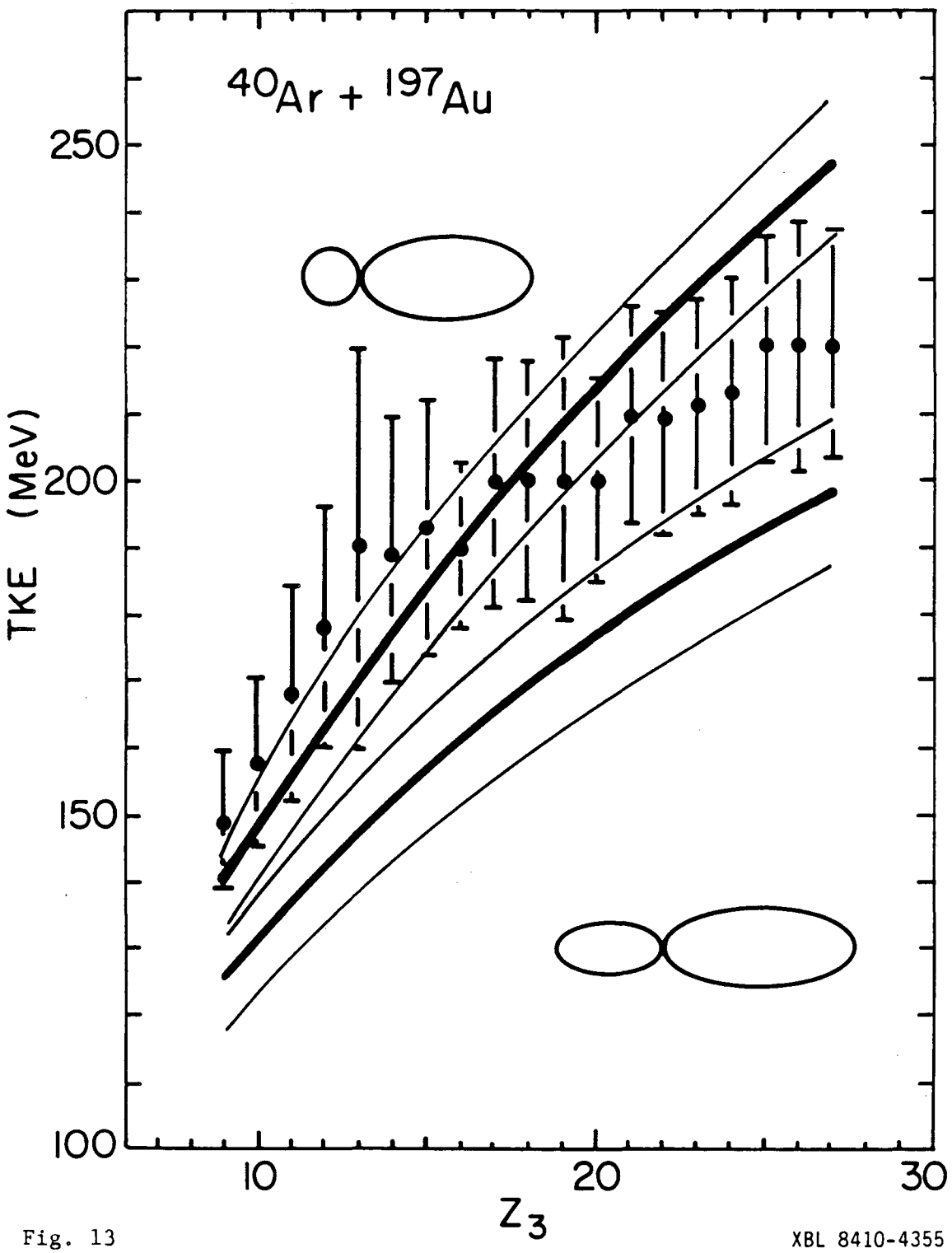

Fig. 13

XBL 8410-4355

This report was done with support from the Department of Energy. Any conclusions or opinions expressed in this report represent solely those of the author(s) and not necessarily those of The Regents of the University of California, the Lawrence Berkeley Laboratory or the Department of Energy.

Reference to a company or product name does not imply approval or recommendation of the product by the University of California or the U.S. Department of Energy to the exclusion of others that may be suitable.

TECHNICAL INFORMATION DEPARTMENT
LAWRENCE BERKELEY LABORATORY
UNIVERSITY OF CALIFORNIA
BERKELEY, CALIFORNIA 94720